Inorganic Chemistry

Article

pubs.acs.org/IC

Synthesis, Structure, Chemical Bonding, and Magnetism of the Series $RELiGe_2$ (RE = La−Nd, Sm, Eu)

Svilen Bobev,* Tae-Soo You,† and Nian-Tzu Suen

Department of Chemistry and Biochemistry, University of Delaware, Newark, Delaware 19716, United States

Shanta Saha, Richard Greene, and Johnpierre Paglione

Department of Physics, University of Maryland, College Park, Maryland 20742, United States

Supporting Information

ABSTRACT: This article focuses on the synthesis and the crystal chemistry of six members of a series of rare-earth metal based germanides with general formula $RELiGe_2$ (RE = La−Nd, Sm, and Eu). The structures of these compounds have been established by single-crystal X-ray diffraction ($CaLiSi_2$ structure type, space group $Pnma$, Z = 4, Pearson symbol $oP16$). The chemical bonding within this atomic arrangement can be rationalized in terms of anionic germanium *zigzag* chains, conjoined via chains of edge-shared $LiGe_4$ tetrahedra and separated by rare-earth metal cations. The structure can also be viewed as an intergrowth of AlB_2-like and TiNiSi-like fragments, or as the result of the replacement of 50% of the rare-earth metal atoms by lithium in the parent structure of the REGe monogermanides. Except for $LaLiGe_2$ and $SmLiGe_2$, the remaining four $RELiGe_2$ phases exhibit Curie−Weiss paramagnetism above about 50 K. In the low temperature regime, the localized 4f electrons in $CeLiGe_2$, $PrLiGe_2$, and $SmLiGe_2$ order ferromagnetically, while antiferromagnetic ordering is observed for $NdLiGe_2$ and $EuLiGe_2$. The calculated effective magnetic moments confirm RE^{3+} ground states in all cases excluding $EuLiGe_2$, in which the magnetic response is consistent with Eu^{2+} configuration ($J = S = 7/2$). The experimental results have been complemented by tight-binding linear muffin-tin orbital (TB-LMTO) band structure calculations.

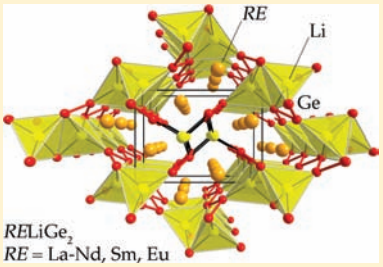

INTRODUCTION

In the past several years, our group has successfully synthesized and characterized numerous types of rare-earth and/or alkaline-earth metal germanides with novel structures.[1−11] In addition to some relatively simple binaries,[2,4,5] examples with more intricate bonding include the ternary RE_2InGe_2,[1] and $RE_{5-x}Mg_xGe_4$ ($1 \le x \le 2.3$) phases (RE = rare-earth metal),[7] RE_2MgGe_2,[11] the homologous series $A_{2[n+m]}In_{2n+m}Ge_{2[n+m]}$ (A = Ca, Sr, Eu, and Yb),[8] $(Sr_{1-x}Ca_x)_5In_3Ge_6/(Eu_{1-x}Yb_x)_5In_3Ge_6$ ($x \approx 0.7$) and $(Sr_{1-x}Ca_x)_3In_2Ge_4/(Sr_{1-x}Yb_x)_3In_2Ge_4$ ($0.4 \le x \le 0.5$),[10] among others. The Ge atoms in most of these structures are either dimerized into Ge dumbbells (formally $[Ge_2]^{6-}$) or "polymerized" into one-dimensional (1-D) chains (formally $^1_\infty[Ge_2]^{q-}$); the latter being an alternation of cis- and trans-Ge−Ge bonds with partial π-delocalization of the Ge 4p-orbitals (hence the fractional formal charge on the 2-bonded germanium atoms). Surveying the recent literature, we found similar Ge chains in several, predominantly Li-containing compounds, such as α-Sr_2LiGe_3,[12] Eu_2LiGe_3,[13] $A_2(Li_{1-x}Mg_x)_2Ge_3$ (A = Sr, Eu; $x \approx 0.5$),[14] $ALiGe_2$ (A = Sr, Ba),[15] $RELiGe_2$ (RE = La−Nd, Sm, and Eu),[16] to name a few. In all of these instances, the small size and the relatively high electronegativity of Li, that is, its ability to form bonds with a partial covalent character, have been suggested as an explanation for the existence of such chains with varied electron count. Further studies on the $ALi_{1-x}In_xGe_2$ ($0 \le x \le 0.1$) and $A_2(Li_{1-x}In_x)_2Ge_3$ ($x \approx 0.3$) phases (A = Sr, Ba, Eu)[9] confirmed the above point, and demonstrated the potential for structural diversity brought up by the special characteristics of the Li metal.

In this article, we report more "lithium chemistry" within the realm of rare-earth metal based germanides by discussing the synthetic efforts and the single-crystal structures of the $RELiGe_2$ (RE = La−Nd, Sm, and Eu) phases, dubbed for short the "1-1-2" compounds. A short analysis of the bonding and the structural trends across the series is also presented. A theoretical treatment of the Ge−Ge bonding within the Ge chains, using the tight-binding linear muffin-tin orbital (LMTO) method, is discussed as well.

EXPERIMENTAL SECTION

Synthesis. All reactions were carried out in welded Nb-ampules. Because of the air-sensitivity of some of the starting materials (pure elements from Alfa or Aldrich (>99.9 wt %)), handling was done inside an argon-filled glovebox or under vacuum. Mixtures of the metals in the desired stoichiometric ratios (1: 1: 2) were loaded into Nb-tubes, which were then sealed by arc-melting under an argon atmosphere. To prevent oxidation upon heating to high temperature, the welded Nb-tubes were subsequently enclosed in fused silica tubes, which were then evacuated (below discharge) and flame-sealed.

Received: October 4, 2011
Published: December 6, 2011

   dx.doi.org/10.1021/ic2021484 | *Inorg. Chem.* 2012, 51, 620−628

Table 1. Selected Crystal Data and Structure Refinement Parameters for *RE*LiGe$_2$ (*RE* = La−Nd, Sm, Eu)

formula	$LaLiGe_2$	$CeLiGe_2$	$PrLiGe_2$	$NdLiGe_2$	$SmLiGe_2$	$EuLiGe_2$
fw/g·mol^{-1}	291.03	292.24	293.03	296.36	302.47	304.08
T/ °C			−73 ± 2			
radiation, wavelength			Mo−Kα, 0.71073 Å			
space group			*Pnma* (No. 62); Z = 4			
unit cell dimensions						
a/ Å	7.8401(12)	7.816(3)	7.7846(6)	7.773(3)	7.7638(5)	8.0735(7)
b/ Å	4.0061(6)	3.9721(15)	3.9509(3)	3.9361(14)	3.9014(3)	3.9730(3)
c/ Å	10.8755(17)	10.757(4)	10.6870(8)	10.644(4)	10.5243(7)	11.0099(9)
V/ Å^3	341.61(9)	333.9(2)	328.69(4)	325.6(2)	318.78(4)	352.5(3)
ρ_{calc}/ g·cm^{-3}	5.659	5.813	5.922	6.045	6.302	5.719
$\mu_{Mo\ K\alpha}$/ cm^{-1}	294.63	309.78	324.47	337.3	365.93	341.63
final R indices [a] [$I > 2\sigma_{(I)}$]	R_1 = 0.0179	R_1 = 0.0212	R_1 = 0.0176	R_1 = 0.0142	R_1 = 0.0144	R_1 = 0.0141
	wR_2 = 0.0402	wR_2 = 0.0453	wR_2 = 0.0383	wR_2 = 0.0345	wR_2 = 0.0327	wR_2 = 0.0295
final R indices [a] [all data]	R_1 = 0.0220	R_1 = 0.0249	R_1 = 0.0197	R_1 = 0.0148	R_1 = 0.0153	R_1 = 0.0129
	wR_2 = 0.0413	wR_2 = 0.0477	wR_2 = 0.0390	wR_2 = 0.0349	wR_2 = 0.0331	wR_2 = 0.0291
largest diff. peak and hole/ e$^-$ Å^{-3}	1.002, −1.025	0.994, −1.037	1.007, −0.975	0.626, −0.745	0.732, −1.232	1.053, −0.678

[a] $R_1 = \sum||F_o| - |F_c||/\sum|F_o|$; $wR_2 = [\sum w(F_o^2 - F_c^2)^2]/\sum w(F_o^2)^2]^{1/2}$, and $w = 1/[\sigma^2F_o^2 + (AP)^2 + BP]$, $P = (F_o^2 + 2F_c^2)/3$; A and B are weight coefficients.

The reaction mixtures containing La, Ce, Pr, and Eu were heated in a tube furnace to 985 °C (rate of 200 °C/h), whereas those containing Nd and Sm were heated to 1085 °C at the same rate. The increase of the reaction temperature was deemed necessary because the melting points of Nd (1021 °C) and Sm (1074 °C) are higher than those of the rest of the early lanthanides.[17] The silica ampules were slowly rotated several times at the melting temperature to ensure homogeneity. All reactions were kept at the maximum temperatures for 5 h, and then cooled at varied steps to ambient temperature (vide infra). The products of such reactions were typically small silver−metallic crystals with irregular shapes. We note here that reactions containing La and Ce produced the purest products when they were slowly cooled down to 600 °C (rate of 10 °C/h) and then brought to room temperature by turning the furnace off. Under the same conditions the reactions containing Pr, Nd, and Eu generated mixtures of the "1-1-2" and the "2-2-3" phase ($Ce_2Li_2Ge_3$ structure type)[18] with a small amount of elemental Ge remaining. The targeted "1-1-2" phase was obtained as single-phase material when the slow cooling step was extended to 300 °C. For all reactions, no additional annealing procedure was needed to improve crystallinity. All products appeared to be stable upon exposure to air and moisture for at least three weeks.

The undertaken elaborate synthetic efforts confirm earlier work (via arc-melting)[16] that the *RE*LiGe$_2$ series spans only the early/midearly rare-earth metals La, Ce, Pr, Nd, and Sm (as well as the nominally divalent Eu and Yb). From the alkaline-earth metals, only Ca forms a compound with this structure,[19] which suggests that the metal's atomic size is the decisive factor for the realization of this structure.

Caution! *Mixtures of the above-discussed elements heated in Nb tubes to 1000 °C and higher temperatures could be dangerous. At these conditions, Nb and Ge could react, causing Li vapors (and molten metals) to leak into the silica tubes. Therefore, the latter must be made sufficiently long, so that one of the ends can be left protruding outside the furnace. In this way, should a leak occur, a condensation at the end of the silica tube would indicate that the furnace must be stopped immediately.*

Crystal Structure Determination. All six compounds were characterized by both powder and single crystal X-ray diffraction. X-ray powder diffraction patterns were collected on a Rigaku MiniFlex powder diffractometer using Cu Kα radiation. The diffractometer was operated at room temperature. The data were gathered in θ−θ scans with a step size of 0.05° in the range of 10° ≤ 2θ ≤ 85° (rate 10 s/step). JADE 6.5 was used for data analysis, which indicated that the observed peaks' positions and intensities were in very good agreement with the simulated patterns.

Single-crystal X-ray diffraction experiments were carried out on a Bruker SMART CCD-based diffractometer. The diffractometer was operated at 200 K, attained through evaporating liquid nitrogen. Monochromated Mo $K\alpha_1$ radiation (λ = 0.71073 Å) was used, and data collections were handled in batch runs at different ω and ϕ angles. Many crystals from each sample were selected and checked by rapid scans before the best ones were found. For the crystals chosen for further analysis, full spheres of intensity data were gathered in batch runs with frame width of 0.3° in ω and θ and data acquisition rate of 10 s/frame. The automated process was controlled by the Bruker SMART software;[20] the SAINT program[21] was used for raw data reduction and extraction of the observed structure factors. Semi-empirical absorption correction based on equivalents was applied using SADABS.[22] Intensity statistics and space group determination were done by the subprogram XPREP in the SHELXTL software package.[23] Subsequently, the structures were solved by direct methods and refined to convergence by full matrix least-squares methods on F^2. Refined parameters included the scale factors, the atomic positions with anisotropic displacement parameters (excluding Li), and extinction coefficients (where applicable). The final difference Fourier maps in all six cases were featureless.

In the last refinement cycles, the atomic positions were standardized by employing STRUCTURE TIDY.[24] Important crystallographic data, atomic positions, selected interatomic distances, and thermal displacement parameters of the series are listed in Tables 1−3. CIFs have also been deposited with Fachinformationszentrum Karlsruhe, 76344 Eggenstein-Leopoldshafen, Germany (fax: (49) 7247-808-666; e-mail: crysdata@fiz.karlsruhe.de), depository numbers CSD-423555 for $LaLiGe_2$; CSD-423556 for $CeLiGe_2$; CSD-423557 for $PrLiGe_2$; CSD-423558 for $NdLiGe_2$; CSD-423559 for $SmLiGe_2$; and CSD-423560 for $EuLiGe_2$. The crystal structures of several *RE*Ge monogermanides, which from a survey of the Inorganic Crystal Structure Database (ICSD) appeared to have been inadequately established, were also reassessed as a part of this study; these details are provided as Supporting Information. The corresponding depository numbers are as follows: CSD-423561 for HT-LaGe (FeB structure type); CSD-423562 for LT-LaGe (LaSi structure type); CSD-423563 for EuGe; CSD-423564 DyGe; CSD-423565 for ErGe; and CSD-423566 for TmGe, respectively.

Magnetic Susceptibility Measurements. Field cooled (FC) and zero field cooled (ZFC) direct current (*dc*) magnetic susceptibility measurements were carried out using either a Physical Property Measurement System (PPMS) or Magnetic Property Measurement System (MPMS) SQUID magnetometer, both by Quantum Design. The measurements were performed in the interval from 2 to 300 K in an applied magnetic field (H) of 100, 500, 1000, or 10000 Oe. The samples (typically 40−100 mg) were loaded in gel caps wrapped with Kapton tape. To ensure reproducibility, specimens from at least two

dx.doi.org/10.1021/ic2021484 | *Inorg. Chem.* 2012, 51, 620−628

Table 2. Atomic Coordinates and Equivalent Isotropic Displacement Parameters (U_{eq} [a]) for *RE*LiGe$_2$ (*RE* = La–Nd, Sm, Eu)

atom	site	*x*	*y*	*z*	U_{eq} (Å^2)
			LaLiGe$_2$		
La	4*c*	0.1412(1)	1/4	0.3664(1)	0.007(1)
Li	4*c*	0.4953(16)	1/4	0.6141(10)	0.016(3)
Ge1	4*c*	0.1590(1)	1/4	0.6811(1)	0.008(1)
Ge2	4*c*	0.2174(1)	1/4	0.0700(1)	0.008(1)
			CeLiGe$_2$		
Ce	4*c*	0.1405(1)	1/4	0.3656(1)	0.007(1)
Li	4*c*	0.4928(16)	1/4	0.6106(12)	0.007(3)
Ge1	4*c*	0.1571(1)	1/4	0.6828(1)	0.008(1)
Ge2	4*c*	0.2218(1)	1/4	0.0689(1)	0.009(1)
			PrLiGe$_2$		
Pr	4*c*	0.1406(1)	1/4	0.3653(1)	0.006(1)
Li	4*c*	0.4924(14)	1/4	0.6092(10)	0.011(2)
Ge1	4*c*	0.1558(1)	1/4	0.6832(1)	0.007(1)
Ge2	4*c*	0.2232(1)	1/4	0.0682(1)	0.007(1)
			NdLiGe$_2$		
Nd	4*c*	0.1403(1)	1/4	0.3651(1)	0.006(1)
Li	4*c*	0.4916(11)	1/4	0.6097(8)	0.011(2)
Ge1	4*c*	0.1547(1)	1/4	0.6838(1)	0.006(1)
Ge2	4*c*	0.2243(1)	1/4	0.0673(1)	0.007(1)
			SmLiGe$_2$		
Sm	4*c*	0.1394(3)	1/4	0.3642(1)	0.008(1)
Li	4*c*	0.4876(12)	1/4	0.6076(9)	0.013(2)
Ge1	4*c*	0.1530(1)	1/4	0.6852(1)	0.009(1)
Ge2	4*c*	0.2277(1)	1/4	0.0658(1)	0.009(1)
			EuLiGe$_2$		
Eu	4*c*	0.1358(1)	1/4	0.3658(1)	0.009(1)
Li	4*c*	0.4973(12)	1/4	0.6130(8)	0.018(2)
Ge1	4*c*	0.1659(1)	1/4	0.6776(1)	0.009(1)
Ge2	4*c*	0.2244(1)	1/4	0.0666(1)	0.009(1)

[a] U_{ij} is defined as one-third of the trace of the orthogonalized U^{ij} tensor.

different reaction batches were measured. The derived net effective moments are listed in Table 4.

Table 4. Relevant Parameters Derived from Linear Fits of the Inverse Susceptibility $\chi(T)^{-1}$ in the Range from 100–300 K for *RE*LiGe$_2$ (*RE* = La–Nd, Sm, Eu)

compounds	magnetic ordering	$[J(J+1)]^{1/2}$	μ_{eff} (μ_B)	θ_p (K)	T_C (K)	T_N (K)
LaLiGe$_2$	Pauli paramagnetic	0	0			
CeLiGe$_2$	FM	2.54	2.78	15(1)	11(1)	
PrLiGe$_2$	FM	3.58	3.82	41(1)	18(1)	
NdLiGe$_2$	AFM	3.62	3.74	13(1)	9(1)	13(1)
SmLiGe$_2$[a]	FM	0.84	0.7	10(1)	22(1)	5(1)
EuLiGe$_2$	AFM	7.94	8.07	−4(1)		26(1)

[a] The net effective moment for Sm^{3+} in SmLiGe$_2$ is derived by a nonlinear fit to the modified Curie–Weiss law.

Computational Details. Tight-binding, linear muffin-tin orbital (TB-LMTO) calculations were carried out in the atomic sphere approximation (ASA) using the LMTO47 program.[25] Exchange and correlation were treated by the local density approximation (LDA).[26] All relativistic effects except spin–orbit coupling were taken into account by using a scalar relativistic approximation. In the ASA method, space is filled with overlapping Wigner–Seitz (WS) atomic spheres.[27] The symmetry of the potential is considered spherical inside each WS sphere, and a combined correction is used to take into account the overlapping part. The radii of WS spheres were obtained by requiring that the overlapping potential be the best possible approximation to the full potential, and were determined by an automatic procedure. This overlap should not be too large because the error in kinetic energy introduced by the combined correction is proportional to the fourth power of the relative sphere overlap. No empty spheres were used. The WS radii are as follows: for LaLiGe$_2$, La = 2.18 Å, Ge1 = 1.48 Å, Ge2 = 1.48 Å, and Li = 1.52 Å; for EuLiGe$_2$, Eu = 2.23 Å, Ge1 = 1.44 Å, Ge2 = 1.44 Å, and Li = 1.59 Å. The basis sets included 6s, 6p, 5d, and 4f orbitals for La; 6s, 6p, 5d, and 6f orbitals for Eu; 4s, 4p, and 4d orbitals for Ge; and 2s, 2p, and 3d orbitals for Li. The La 6p, Eu 6p, Ge 4d, and Li 2p and 3d orbitals

Table 3. Important Interatomic Distances (Å) for *RE*LiGe$_2$ (*RE* = La–Nd, Sm, Eu)

LaLiGe$_2$		CeLiGe$_2$		PrLiGe$_2$	
atomic pair	distance	atomic pair	distance	atomic pair	distance
Ge1–Ge2 (×2)	2.5318(8)	Ge1–Ge2 (×2)	2.5180(10)	Ge1–Ge2 (×2)	2.5109(7)
Li–Ge1	2.582(14)	Li–Ge1	2.563(13)	Li–Ge1	2.561(12)
Li–Ge2	2.643(10)	Li–Ge2	2.632(13)	Li–Ge2	2.615(12)
La–Ge1 (×2)	3.1335(8)	Ce–Ge1 (×2)	3.1034(11)	Pr–Ge1 (×2)	3.0812(7)
La–Ge1 (×2)	3.2454(8)	Ce–Ge1 (×2)	3.2111(11)	Pr–Ge1 (×2)	3.1944(7)
La–Ge2 (×2)	3.1847(7)	Ce–Ge2 (×2)	3.1435(11)	Pr–Ge2 (×2)	3.1183(6)
La–Ge2	3.2788(10)	Ce–Ge2	3.2546(15)	Pr–Ge2	3.2410(8)
La–La (×2)	4.0061(6)	Ce–Ce (×2)	3.9721(15)	Pr–Pr (×2)	3.9509(3)
La–La (×2)	4.1661(7)	Ce–Ce (×2)	4.1389(11)	Pr–Pr (×2)	4.1199(5)
NdLiGe$_2$		SmLiGe$_2$		EuLiGe$_2$	
atomic pair	distance	atomic pair	distance	atomic pair	distance
Ge1–Ge2 (×2)	2.5088(8)	Ge1–Ge2 (×2)	2.4986(5)	Ge1–Ge2 (×2)	2.4948(5)
Li–Ge1	2.537(9)	Li–Ge1	2.531(10)	Li–Ge1	2.678(9)
Li–Ge2	2.611(9)	Li–Ge2	2.606(6)	Li–Ge2	2.697(9)
Nd–Ge1 (×2)	3.0659(9)	Sm–Ge1 (×2)	3.0376(5)	Eu–Ge1 (×2)	3.1791(5)
Nd–Ge1 (×2)	3.1839(8)	Sm–Ge1 (×2)	3.1553(5)	Eu–Ge1 (×2)	3.2865(5)
Nd–Ge2 (×2)	3.1007(8)	Sm–Ge2 (×2)	3.0608(5)	Eu–Ge2 (×2)	3.1793(4)
Nd–Ge2	3.2359(13)	Sm–Ge2	3.2152(7)	Eu–Ge2	3.3709(6)
Nd–Nd (×2)	3.9361(14)	Sm–Sm (×2)	3.9014(3)	Eu–Eu (×2)	3.9730(3)
Nd–Nd (×2)	4.1084(10)	Sm–Sm (×2)	4.0813(4)	Eu–Eu (×2)	4.1818(4)

dx.doi.org/10.1021/ic2021484 | *Inorg. Chem.* 2012, 51, 620–628

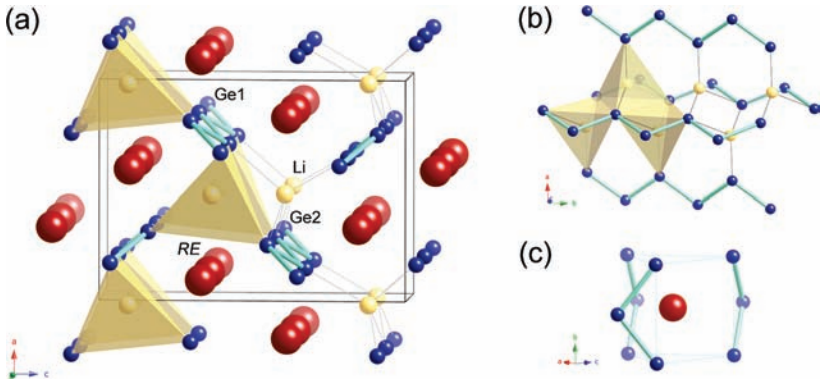

Figure 1. (a) Combined polyhedral and ball-and-stick representations of the orthorhombic structure of *RE*LiGe$_2$ (*RE* = La–Nd, Sm, and Eu). The unit cell is outlined. The *RE* atoms are shown as dark-red spheres, and the Ge atoms are drawn as blue spheres. The Li atoms (in yellow) are shown as the centers of translucent LiGe$_4$ tetrahedra or as yellow spheres connected to four neighboring Ge atoms. The $^1_\infty$[Ge$_2$] chains are emphasized. (b) Expanded view of the $^1_\infty$[Ge$_2$] chains and the edge-sharing mode of the LiGe$_4$ tetrahedra. (c) Expanded view of the coordination polyhedron of the *RE* atoms.

were treated by the Löwdin downfolding technique;[27] the Eu 4f wave functions were treated as core functions occupied by 7 electrons. This assigns the Eu atoms as formally Eu(II), which is consistent with the results of the magnetic susceptibility measurements. To evaluate various interatomic orbital interactions, the crystal orbital Hamilton populations (COHP)[28] curves and the integrated COHP values (ICOHPs) were also calculated. The *k*-space integrations were conducted by the tetrahedron method, and the self-consistent charge density was obtained using 192 irreducible *k*-points in the Brillouin zone.

RESULTS AND DISCUSSION

Structure. The *RE*LiGe$_2$ (*RE* = La–Nd, Sm, and Eu) phases have been identified previously from their powder X-ray diffraction patterns[16] as crystallizing with the CaLiSi$_2$ structure type[19] (space group *Pnma*; Pearson code *oP*16).[29] Our single-crystal work confirms this classification and for the first time provides accurate refinements of the atomic positions.

The structure, as seen in Figure 1, is not complicated, and can be readily described. The most prominent aspect of the structure is the *zigzag* $^1_\infty$[Ge$_2$] chain. These 1-D polyanions propagate parallel to the crystallographic *b*-axis and are linked together via chains of edge-shared LiGe$_4$-tetrahedra, also running in the same direction. Emphasizing the covalency of the Li–Ge bonding, the structure can also be rationalized as a polyanionic $^3_\infty$[LiGe$_2$] network, with rare-earth metal cations residing in the channels within it.

Besides the title *RE*LiGe$_2$ (*RE* = La–Nd, Sm, Eu) compounds and YbLiGe$_2$,[30] other rare-earth metal lithium germanides with similar formula exist, such as EuLi$_{0.9}$In$_{0.1}$Ge$_2$.[9] However, the topology of the $^1_\infty$[Ge$_2$] chains in the structures in question is different: the former structure has chains with *zigzag* connectivity (i.e., Ge–Ge bonds alternating in trans-fashion), while the latter boasts a repeating unit of both the cis- and trans-conformations. The similarities and the differences between the two arrangements can be explained once their close connection to some other known structures is realized (Figure 2). More specifically, as described by us in a recent paper,[9] the "1-1-2" phases can be considered as derivatives of the hypothetical *RE*Ge$_2$ compounds (AlB$_2$ structure type). This idea is schematically represented in Figure 2, where the honeycomb $^2_\infty$[Ge$_2$] layers in the parent AlB$_2$-type structure are "cut" to either *zigzag* (trans–trans) or cis–trans $^1_\infty$[Ge$_2$] chains by cleaving selected Ge–Ge bonds. This imaginary process can account for the polymorphic

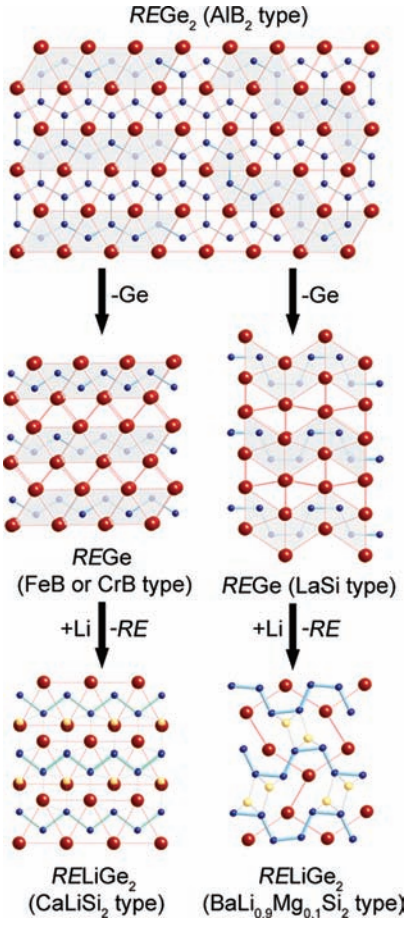

Figure 2. Schematic representation of the structural relationship between the hypothetical *RE*Ge$_2$ (*RE* = La–Nd, Sm and Eu) compounds with the AlB$_2$ structure type and the corresponding *RE*Ge monogermanides (FeB, CrB, or LaSi structure types). A formal substitution of 1/2 of the *RE* atoms in the latter structures with Li yields two different *RE*LiGe$_2$ structures, with different $^1_\infty$[Ge$_2$] chains, either with *zigzag* connectivity (i.e., Ge–Ge bonds alternating in *trans*-fashion) or with a repeating unit of both the cis- and trans-conformations. See text for details.

structures of the monogermanides *RE*Ge (FeB, CrB, or LaSi structure types).[31] In the next step, a "substitution" of 1/2 of

dx.doi.org/10.1021/ic2021484 | *Inorg. Chem.* 2012, 51, 620–628

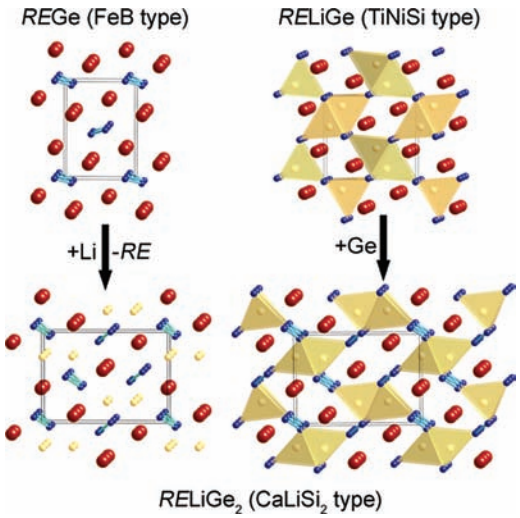

Figure 3. Schematic representation of the structural relationship between the *RE*Ge (FeB structure type), *RE*LiGe (TiNiSi structure type), and the title *RE*LiGe$_2$ compounds (CaLiGe$_2$ structure type). The three structures have the same extended symmetry and share the positions of the *RE* atoms. See text for details.

the rare-earth metals atoms with Li in the structure of each monogermanide yields the two different "1-1-2" structures.

The topological relation of the structure of *RE*LiGe$_2$ (*RE* = La–Nd, Sm, and Eu) to that of the *RE*Ge phases (*RE* = La–Pr)[31] crystallizing with the FeB structure type is useful to note and is schematically presented in Figure 3. The same illustration also shows that the *RE*LiGe$_2$ compounds can be considered as close relatives of the hypothetical *RE*LiGe germanides with the TiNiSi structure type[32] (aka SrMgSi): a simple "insertion" of another germanium atom and an appropriate resizing of the unit cell accounts for the above-mentioned polyanionic $^{3}_{\infty}$[LiGe$_2$] network. Notably, the three depicted structures share not only the same arrangement of rare-earth metal atoms, but the same symmetry as well (*Pnma*).

The analogy with the FeB structure type can be used to rationalize the inability to extend the *RE*LiGe$_2$ series beyond Eu (see Experimental Section). It is known that the FeB structure type is common among the early rare-earth metals, whereas the late rare-earth metals form *RE*Ge with the CrB structure type, with polymorphic transitions between the two for the middle members of the 4f-block.[31] This phenomenology has been attributed to the lanthanide contraction and the decreasing size of the rare-earth metals. Indeed, we observe that as the atomic sizes of the lanthanides gradually decreases from La to Sm (r_{La} = 1.69 Å, r_{Ce} = 1.65 Å, r_{Pr} = 1.64 Å, r_{Nd} = 1.63 Å, and r_{Sm} = 1.62 Å),[33] the lattice parameters monotonically decrease (Table 1). These changes in the unit cell constants correlate with the refined Ge–Ge distances in the $^{1}_{\infty}$[Ge$_2$] chains, which show a gradual decrease from 2.5318(8) Å for LaLiGe$_2$ to 2.4986(5) Å for SmLiGe$_2$, respectively (Table 3). The corresponding Ge–Ge–Ge angles decreases as well from 104.58(3)° to 102.67(3)° for LaLiGe$_2$ and SmLiGe$_2$, respectively.

The unit cell volume for EuLiGe$_2$ is larger than the rest because of the existence of europium as Eu(II), which results in the enlarged atomic radius (r_{Eu} = 1.85 Å).[33] However, the increased unit cell volume does not correspond to a longer Ge–Ge distance, as one could expect if the trends were followed. In fact, the Ge–Ge distance in EuLiGe$_2$ is the shortest of all, 2.4948(5) Å. Such bond length compares well with those reported for other compounds with polyene-like $^{1}_{\infty}$[Ge$_2$] chains, such as α-Sr$_2$LiGe$_3$,[12] Eu$_2$LiGe$_3$,[13] A_2(Li$_{1-x}$Mg$_x$)$_2$Ge$_3$ (*A* = Sr, Eu),[14] *A*LiGe$_2$ (*A* = Sr, Ba),[15] and *A*Li$_{1-x}$In$_x$Ge$_2$ and A_2(Li$_{1-x}$In$_x$)$_2$Ge$_3$ (*A* = Sr, Ba, Eu).[9] In all of the above cases, the Ge–Ge bonds in the chains are slightly shorter than what can be considered 2-center 2-electron Ge–Ge bonds. Some examples here include the Ge–Ge bonding in the puckered layers in CaGe$_2$ (d_{Ge-Ge} = 2.5417(7)–2.5513(7) Å),[5] and EuGe$_2$ (d_{Ge-Ge} = 2.564(4) Å),[34] in the [Ge$_4$] clusters in BaGe$_2$ and K$_4$Ge$_4$ (average d_{Ge-Ge} = 2.55–2.56 Å),[35] and in the [Ge$_2$] dumbbells in Ca$_5$Ge$_3$ (d_{Ge-Ge} = 2.575(1) Å,[36] among many others.

We must also note that similar *zigzag* $^{1}_{\infty}$[Ge$_2$] chains are present in all *RE*Ge phases (either FeB or CrB-type structures). However, the structures of many monogermanides appear inadequately studied and the published crystallographic data cannot be deemed reliable by today's standards. For example, we repeated the synthesis of the LaGe HT-polymorph (FeB-type), and refined its structure; the hereby determined Ge–Ge distance is 2.676(1) Å, not 2.509 Å as in the literature.[31] Large discrepancies were also found for DyGe (d_{Ge-Ge} = 2.678(3) Å, instead of the published 2.546 Å [31]); and TmGe (d_{Ge-Ge} = 2.639(3) Å instead of the published 2.571 Å[31]). For detailed crystallographic data on *RE*Ge, we refer the reader to the Supporting Information section. Because of these problems, a direct comparison of the structural trends among the monogermanides and the title compounds is hampered, although apparent correlations do exist. Most notably, it is clear that the refined Ge–Ge distances in all *RE*LiGe$_2$ are significantly shorter than the Ge–Ge distances in the corresponding *RE*Ge monogermanides. These nuances of the Ge–Ge bonding are further discussed below and in the electronic calculation section.

The apparent contraction of the Ge–Ge bonds in *RE*LiGe$_2$ versus *RE*Ge (=*RE*$_2$Ge$_2$) series indicate an electronic effect at play here since the structural features in both families are subtly influenced by the available valence electrons. The simplest approach toward the electron count, the Zintl–Klemm formalism,[37] calls for a formulation [*RE*$^{3+}$][Li^{+}][Ge^{2-}]$_2$, whereby each 2-bonded Ge atom in the *zigzag* chain is assigned a formal charge 2– to satisfy the octet rule. Such an electron count is just like in CaGe (e.g., Ca^{2+}Ge^{2-})[38] and EuGe (e.g., Eu^{2+}Ge^{2-}).[39] However, the formal electron count for the remaining *RE*Ge phases with *RE*$^{3+}$ cations yields a more reduced germanium state (viz., *RE*$^{3+}$Ge^{3-}) series. In contrast, EuLiGe$_2$ with Eu^{2+} instead of Eu^{3+} will require a formulation [Eu^{2+}][Li^{+}][Ge$^{1.5-}$]$_2$ (also valid in the cases of CaLiGe$_2$[19] and YbLiGe$_2$[30]), that is, a partial double bond character of the Ge–Ge interactions and some conjugation of the Ge π^* orbitals along the chain must be considered. The shortest Ge–Ge distance in EuLiGe$_2$, which are isostructural (but not isoelectronic) to the *RE*LiGe$_2$ compounds containing trivalent cations was already noted; another example confirming this line of thinking is the fact that CaLiGe$_2$ (formally [Ca^{2+}][Li^{+}][Ge$^{1.5-}$]$_2$)[19] and YbLiGe$_2$ (formally [Yb^{2+}][Li^{+}][Ge$^{1.5-}$]$_2$)[30] also have very short Ge–Ge bonds of 2.490(2) Å and 2.476(2) Å, respectively. Comparing those to LaLiGe$_2$ (d_{Ge-Ge} = 2.5318(8) Å; formally [La^{3+}][Li^{+}][Ge^{2-}]$_2$) and CeLiGe$_2$ (d_{Ge-Ge} = 2.518(1) Å; formally [Ce^{3+}][Li^{+}][Ge^{2-}]$_2$) is instructive since the corresponding Pauling single-bond radii are very close and "size" effects could be ruled out: r_{Ca} = 1.74 Å, r_{Yb} = 1.70 Å, r_{La} = 1.69 Å, and r_{Ce} = 1.65 Å.[33]

The "special" role of lithium in these structures must be briefly discussed too. As mentioned already, here and in some

dx.doi.org/10.1021/ic2021484 | *Inorg. Chem.* 2012, 51, 620–628

earlier publications,[9,10,12−14] the Li atoms can be regarded as both donors of valence electrons to the germanium chains, that is, as cations, and as participants in covalent interactions within the polyanionic $^{3}_{\infty}[LiGe_2]$ network (the structural relationship to TiNiSi structure type; see Figure 3). A closer look at the coordination environment of the Li atoms supports both notions: Li atoms are found in distorted tetrahedra of Ge atoms at distances in the range 2.531(10)−2.697(9) Å. Each Li-centered tetrahedron is edge-shared with two neighboring tetrahedra, forming double-tetrahedral chains (Figure 1 and Figure 3). They propagate parallel to the *c*-axis and are further connected to four neighboring units (in the *ab*-plane) via *zigzag* Ge chains. The reported distances are slightly longer than the sum of the Pauling's single-bond radii (r_{Li} = 1.225 Å; r_{Ge} = 1.242 Å),[33] and compare well with those reported for other lithium germanides, such as Eu_2LiGe_3,[13] $A_2(Li_{1-x}Mg_x)_2Ge_3$ (A = Sr, Eu; $x \approx 0.5$),[14] and $ALiGe_2$ (A = Sr, Ba),[15] $Ce_2Li_2Ge_3$,[18] and $ALi_{1-x}In_xGe_2$ ($0 \le x \le 0.1$) and $A_2(Li_{1-x}In_x)_2Ge_3$ ($x \approx 0.3$) (A = Sr, Ba, Eu).[9] The shortest Li−*RE* distances are greater than 3.5 Å.

The larger lanthanide atoms reside in the "channels" of the $^{3}_{\infty}[LiGe_2]$ network and are surrounded by nine Ge atoms located on three neighboring 1-D *zigzag* chains (Figure 1c). Such coordination polyhedron can be described as a trigonal prism formed by six Ge atoms located within less than 3.25 Å around the central atom, and three additional Ge atoms at distances of 3.28 to 3.42 Å, located in capping positions. The closest *RE*−*RE* contacts are on the order of 3.9−4.2 Å, much longer than the corresponding *RE*−*RE* contacts in the elemental crystal structures.[29]

Electronic Structure. To access the electronic band structures and to investigate the chemical interactions influencing the structural stability and physical properties of the compounds of the $RELiGe_2$ series, TB-LMTO-ASA band structure calculations were carried out using local density approximation (LDA) on two observed and one hypothetical structure. In particular, two refined structures, that of $LaLiGe_2$ and $EuLiGe_2$, were used for the calculations of the 12 valence electron (ve^-) system with trivalent cations (*RE* = La−Sm) and the 11 ve^- system with divalent cations (Ca, Eu, and Yb), respectively. In addition, a model structure of $EuLiGe_2$ adopting the $BaLi_{0.9}Mg_{0.1}Si_2$-type structure was also taken in consideration to compare the energetic stability of the cis−trans versus trans−trans $^{2}_{\infty}[Ge_2]$ chains for systems with identical spatial and electronic characteristics. The results of these studies are presented with the corresponding density of states (DOS) and COHP curves; an analysis of the integrated crystal orbital Hamilton population (COHP) values is discussed as well.

Figure 4(a) shows DOS and COHP curves of $LaLiGe_2$. Overall total DOS (TDOS) displays significant mixing among valence orbitals of La, Li, and Ge, and the largest partial DOS (PDOS) contribution, of course, comes from Ge atoms because of the largest molar ratio in the given composition. Two deep pseudogaps are observed: one is almost at the Fermi level (E_F) which corresponds to 12 ve^-, and the other one is at about 0.4 eV below E_F, corresponding to 11.5 ve^-. The region below E_F is mostly composed of contributions from Ge and Li, whereas the region above E_F consists of mostly La 5d orbital contributions with some small admixture with Li and Ge. The occupied states below E_F can be divided into three segments: (1) a bonding valence band of 2s of Li and 4s of Ge between about 9.5 and 11 eV below E_F; (2) a bonding and an antibonding valence band of 4p of Ge together with a bonding valence band of 2s of Li between 6 and 8.5 below E_F; and (3) a bonding valence band of 2s of Li, 4p of Ge, and 5d of La between about 0 and 4.5 eV below E_F. The Li PDOS displays a considerable participation in covalent interactions within the polyanionic $^{3}_{\infty}[LiGe_2]$ network using 2s orbitals, providing additional evidence for the unique role the Li atoms play in the bonding, as already discussed.

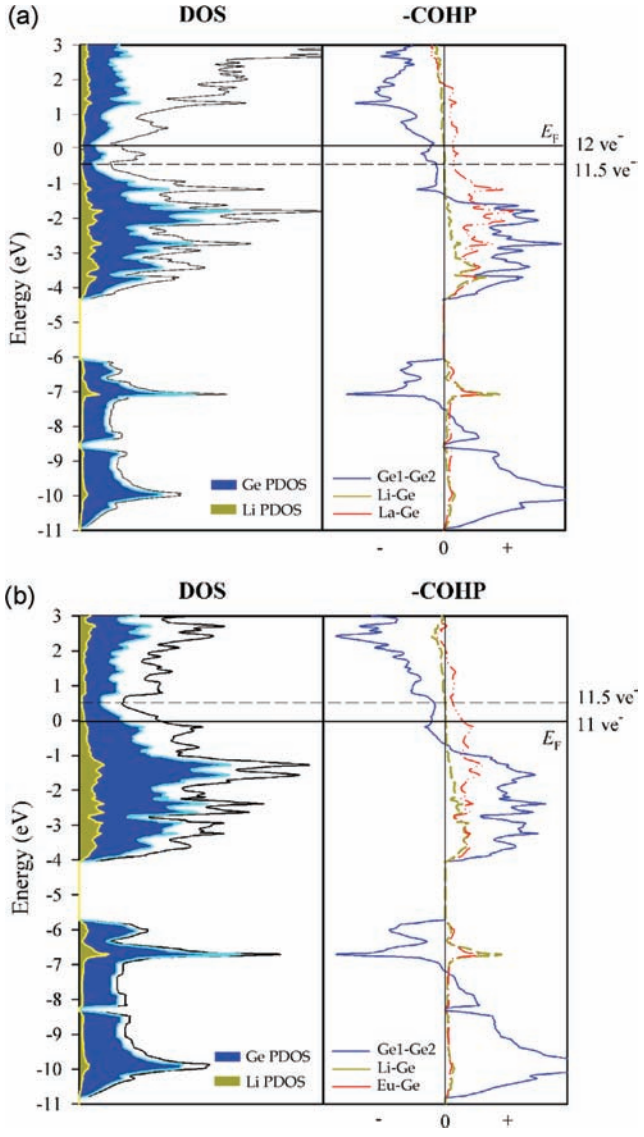

Figure 4. (a) Calculated DOS and COHP of $LaLiGe_2$. (b) Calculated DOS and COHP of $EuLiGe_2$. The total DOS and the partial DOS are plotted on the same energy scale. The actual Fermi level (E_F) is chosen as the energy reference at 0 eV and drawn as a solid line; estimated Fermi level for different valence electron counts are shown with dashed lines.

TDOS and PDOS plots (Figure 4b) of $EuLiGe_2$ are similar, overall, to those of $LaLiGe_2$ including valence orbital mixing of Eu, Li, and Ge throughout all energy levels. However, unlike the system involving a trivalent rare-earth metal, which locates E_F at the pseudogap, E_F of $EuLiGe_2$ corresponding to 11 ve^- is situated about 0.5 eV below a deep local minimum. In addition, TDOS at E_F is relatively high. One could surmise that spin polarization and differences between the majority and minority spins cause an "anomaly", but the corresponding spin-polarized

dx.doi.org/10.1021/ic2021484 | *Inorg. Chem.* 2012, 51, 620−628

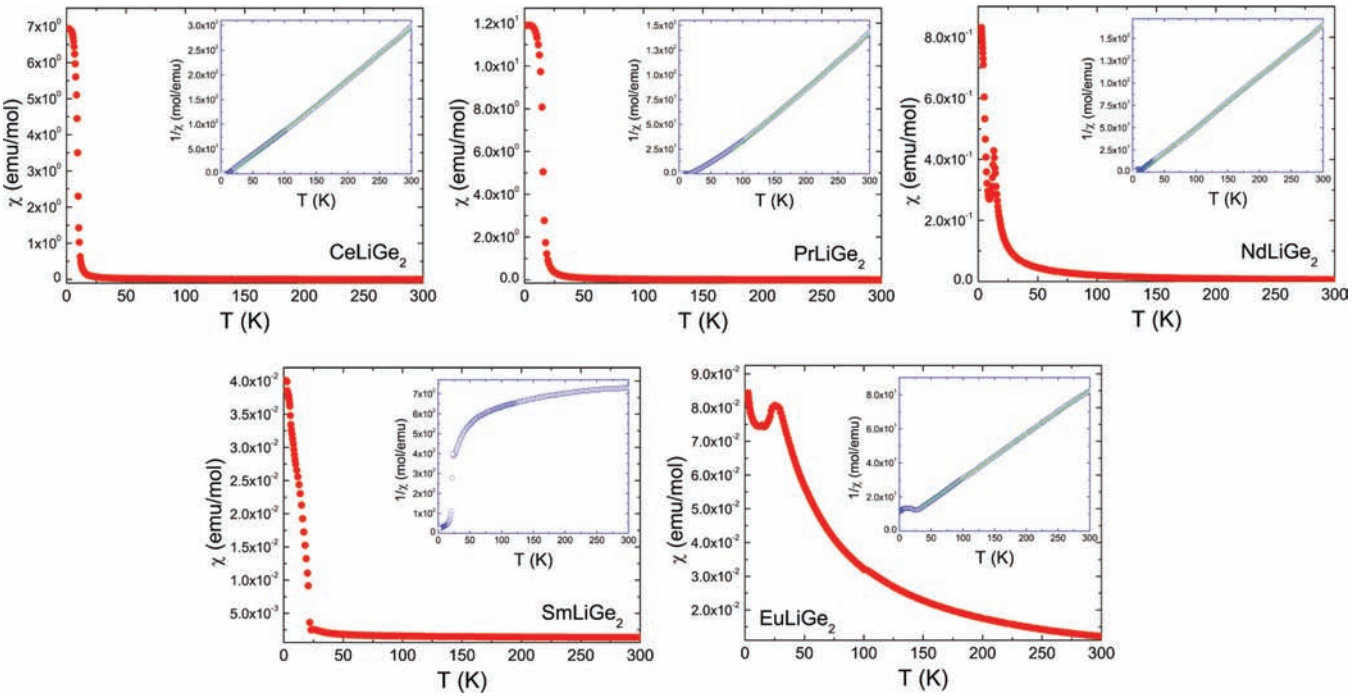

Figure 5. Temperature dependence of the magnetic susceptibility of *RE*LiGe$_2$ (*RE* = Ce–Nd, Sm and Eu). Inset: Inverse susceptibility vs temperature with linear fits to the Curie–Weiss law.

DOS, which is presented in the Supporting Information section clearly rules out such a hypothesis: spin polarization leaves the Ge orbitals (main contributors near the Fermi level) untouched since essentially there is no exchange splitting. Another possibility is that this feature indicates electronic instability, therefore, we checked if another structure, which would be more stable from an electronic structural viewpoint can be adopted by EuLiGe$_2$. A logical choice here was EuLiGe$_2$ ("extrapolated" from $EuLi_{0.91(1)}In_{0.09}Ge_2$[9]) with the $BaLi_{0.9}Mg_{0.1}Si_2$-structure type, whose structure features cis–trans chains. All the details are given in the Supporting Information; we just note that the calculation parameters, WS radii of each atom, number of *k*-points, and the volume of unit cells, were kept identical to those employed for the already discussed calculation of EuLiGe$_2$ with the $CaLiSi_2$-structure type (*zigzag* chains). According to the results, the total electronic energy of the structure with the cis–trans chains is higher (by 971 meV/unit cell) than the structure with *zigzag* chains, rendering this supposition unreasonable.

COHP analyses of the LaLiGe$_2$ (12 ve$^-$) and EuLiGe$_2$ (11 ve$^-$) compounds reveal several interesting features as well. The Ge–Ge bonding in both cases has an antibonding character at E_F, which is easily understood following the in-depth analysis by Mudring and Corbett (the case study of Ca_5Ge_3).[36] However, we note that the antibonding character is smaller in EuLiGe$_2$ than in LaLiGe$_2$, which can be clearly seen from the relatively less populated π^* states in EuLiGe$_2$ compared to LaLiGe$_2$ (Figure 4). Furthermore, the integrated crystal orbital Hamilton population (COHP) values—the ICOHP in EuLiGe$_2$ is 2.86 eV/cell, compared to 2.50 eV/cell in LaLiGe$_2$. Such differences can also be correlated to the relatively shorter Ge–Ge distance in EuLiGe$_2$ (d_{Ge-Ge} = 2.4948(5) Å) versus LaLiGe$_2$ (d_{Ge-Ge} = 2.5318(8) Å), respectively. This means that a partial double-bond character should be ascribed to the Ge–Ge bonding.

The antibonding character of the Ge–Ge bonds in both LaLiGe$_2$ and EuLiGe$_2$ is fully compensated by the relatively strong La–Ge1(Ge2) and Eu–Ge1(Ge2) bonding, which results in overall energetically favorable structures. The COHP curves for the Li–Ge1(Ge2) interactions show they are weaker than the Ge–Ge bonds and exhibit nearly nonbonding character in the proximity of the E_F.

Magnetic Susceptibilities. The temperature dependence of the molar magnetic susceptibilities ($\chi_m = M/H$) of all *RE*LiGe$_2$ (*RE* = Ce–Nd, Sm and Eu) samples are presented in Figure 5. In all cases, polycrystalline specimens were used and *M* was measured between 300 and 1.8 K in field cooling mode; a comparison of the temperature dependent magnetization data in field cooled (FC) and zero field cooled (ZFC) is provided as Supporting Information.

As seen from the figure, in the high temperature regime, CeLiGe$_2$, PrLiGe$_2$, NdLiGe$_2$, and SmLiGe$_2$ display paramagnetic behavior that follows the Curie–Weiss law $\chi(T) = C/(T - \theta_p)$,[40] where *C* is the Curie constant ($N_A\mu_{eff}^2/3k_bT$) and θ_p is the Weiss temperature. The calculated effective magnetic moments (Table 4) are close to the theoretical values of RE^{3+} (*RE* = Ce–Nd),[40] as expected, which indicates magnetic ground states from 4f-electron origin. A Pauli-like paramagnetic ground state exists for LaLiGe$_2$, since the La^{3+} ion has no 4f electrons. The SmLiGe$_2$ specimen shows typical Van Vleck paramagnetism[41] in the high temperature range; in this instance, the significant contribution of the temperature independent term (χ_o) to the molar susceptibility requires a nonlinear fit to the modified Curie–Weiss law, $\chi_m(T) = \chi_o + C/(T - \theta_p)$,[41] to calculate the effective moment for Sm^{3+}. The effective moment determined for the EuLiGe$_2$ sample (8.07 μ_B) is on par with the free-ion value for Eu^{2+} (7.94 μ_B),[41] corroborating the earlier discussions on the crystal and electronic structure.

In the low temperature regime, all compounds in this series (excluding LaLiGe$_2$) undergo magnetic ordering: both CeLiGe$_2$ and PrLiGe$_2$[42] enter into ferromagnetic states (FM) with T_C of

dx.doi.org/10.1021/ic2021484 | *Inorg. Chem.* 2012, 51, 620–628

about 11 and 18 K, respectively. The data on $NdLiGe_2$ show a clear cusp-like feature in both the FC and ZFC magnetization curves, which indicate the onset of antiferromagnetic ordering (AFM) with Néel temperature (T_N) of about 13 K. Below T_N, the susceptibility rises again, hinting at the possibility for a second transition, likely of a ferromagnetic type occurring at about 9 K. The positive Weiss constant of $NdLiGe_2$ (Table 4) also suggests ferromagnetic ordering. The behavior of $SmLiGe_2$ in the low temperature regime is also complicated: from the FC data it appears that the unpaired electrons of the Sm^{3+} ions align in a ferromagnetic fashion with T_C of about 22 K. However, the ZFC data reveal a peak at about 5 K, which is reminiscent of an antiferromagnetically ordered state, followed by a small jump of the susceptibility at T_C. The origin of these transitions is not fully understood yet. $\chi_m(T)$ of $EuLiGe_2$ indicates a straightforward antiferromagnet with a Néel temperature of about 26 K.

Comparing the magnetic ordering in this series with the closely related *RE*Ge monogermanides shows that the early ones (*RE*Ge, *RE* = Pr, Nd) are ordered ferromagnetically, while for the mid-to-late ones (*RE*Ge, *RE* = Tb−Tm), the magnetic ground state is antiferromagnetic. The magnetism in these compounds has been explained by the electrons-mediated coupling (RKKY theory)[40] and the monotonically decreased distance between the *RE* metal atoms on moving across the series.

■ ASSOCIATED CONTENT

Supporting Information

A combined X-ray crystallographic file in CIF format, along with details on the reaccessed crystal structures of some *RE*Ge monogermanides; details on the electronic structure calculations of $EuLiGe_2$ with the $BaLi_{0.9}Mg_{0.1}Si_2$-structure type; results from spin-polarized calculations; table with integrated COHP for selected interactions; plots with $\chi(T)$ for $RELiGe_2$ (*RE* = Ce−Nd, Sm and Eu) measured on FC and ZFC modes; a representative powder X-ray diffraction pattern matched with the calculated one. This material is available free of charge via the Internet at http://pubs.acs.org.

■ AUTHOR INFORMATION

Corresponding Author

*Phone: (302) 831-8720. Fax: (302) 831-6335. E-mail: bobev@udel.edu.

Present Address

[†]Department of Chemistry, Chungbuk National University, Cheongju, Chungbuk, 361−763, South Korea.

■ ACKNOWLEDGMENTS

Svilen Bobev acknowledges financial support from the National Science Foundation through Grant DMR-0743916 (CAREER). Work at UMD was supported by an AFOSR MURI Award (FA955-09-1-0603). Work at CBNU was supported by a research grant from the Chungbuk National University in 2011.

■ REFERENCES

(1) Tobash, P. H.; Lins, D.; Bobev, S.; Lima, A.; Hundley, M. F.; Thompson, J. D.; Sarrao, J. L. *Chem. Mater.* **2005**, *17*, 5567−5573.

(2) (a) Tobash, P. H.; Lins, D.; Bobev, S.; Hur, N.; Thompson, J. D.; Sarrao, J. L. *Inorg. Chem.* **2006**, *45*, 7286−7294. (b) Tobash, P. H.; Bobev, S.; Thompson, J. D.; Sarrao, J. L. *J. Alloys Compd.* **2009**, *488*, 533−537.

(3) Tobash, P. H.; Bobev, S. *J. Am. Chem. Soc.* **2006**, *128*, 3532−3533.

(4) Tobash, P. H.; DiFilippo, G.; Bobev, S.; Hur, N.; Thompson, J. D.; Sarrao, J. L. *Inorg. Chem.* **2007**, *46*, 8690−8697.

(5) Tobash, P. H.; Bobev, S. *J. Solid State Chem.* **2007**, *180*, 1575−1581.

(6) Tobash, P. H.; Meyers, J. J.; DiFilippo, G.; Bobev, S.; Ronning, F.; Thompson, J. D.; Sarrao, J. L. *Chem. Mater.* **2008**, *20*, 2151−2159.

(7) Tobash, P. H.; Bobev, S.; Thompson, J. D.; Sarrao, J. L. *Inorg. Chem.* **2009**, *48*, 6641−6651.

(8) You, T.-S.; Tobash, P. H.; Bobev, S. *Inorg. Chem.* **2010**, *49*, 1773−1783.

(9) You, T.-S.; Bobev, S. *J. Solid State Chem.* **2010**, *183*, 2895−2902.

(10) You, T.-S.; Bobev, S. *J. Solid State Chem.* **2010**, *183*, 1258−1265.

(11) Suen, N.-T.; Tobash, P. H.; Bobev, S. *J. Solid State Chem.* **2011**, *184*, 2941−2947.

(12) Xie, Q.-X.; Reyes, E. C.; Wörle, M.; Nesper, R. *Z. Anorg. Allg. Chem.* **2011**, *637*, 846−858.

(13) (a) Xie, Q.-X.; Nesper, R. *Z. Kristallogr.* **2004**, *219*, 79−80. (b) Xie, Q.-X.; Nesper, R. *Z. Anorg. Allg. Chem.* **2006**, *632*, 1743−1751.

(14) Xie, Q.-X.; Nesper, R. *Z. Kristallogr.* **2004**, *219*, 83−84.

(15) Park, D. G.; Dong, Y.-K.; DiSalvo, F. J. *J. Alloys Compd.* **2009**, *470*, 90−95.

(16) Pavlyuk, V. V.; Pecharskii, V. K.; Bodak, O. I. *Dopov. Akad. Nauk Ukr. RSR, Ser. A* **1986**, *48*, 78−80.

(17) *CRC Handbook of Chemistry and Physics*, 83rd ed.; CRC Press LLC: Boca Raton, FL, 2002.

(18) Pavlyuk, V. V.; Pecharskii, V. K.; Bodak, O. I.; Bruskov, V. A. *Kristallografiya* **1988**, *33*, 46−50.

(19) Müller, W.; Schäfer, H.; Weiss, A. *Z. Naturforsch., B. Anorg. Chem. Organ. Chem.* **1971**, *26*, 534−536.

(20) *SMART, NT*, version 5.63; Bruker Analytical X-ray Systems, Inc.: Madison, WI, 2003.

(21) *SAINT, NT*, version 6.45; Bruker Analytical X-ray Systems, Inc.: Madison, WI, 2003.

(22) *SADABS, NT*, version 2.10; Bruker Analytical X-ray Systems, Inc.: Madison, WI, 2001.

(23) *SHELXTL*, version 6.12; Bruker Analytical X-ray Systems, Inc.: Madison, WI, 2001.

(24) Gelato, L. M.; Parthé, E. *J. Appl. Crystallogr.* **1987**, *20*, 139−146.

(25) Jepsen, O.; Burkhardt, A.; Andersen, O. K. *The TB-LMTO-ASA Program*, version 4.7; Max-Planck-Institut für Festkörperforschung: Stuttgart, Germany, 1999.

(26) von Barth, U.; Hedin, L. *J. Phys. C: Solid State Phys.* **1972**, *5*, 1629−1642.

(27) Andersen, O. K.; Jepsen, O.; Glötzel, D. In *Highlights of Condensed Matter Theory*; Bassani, F., Fumi, F., Tosi, M., Eds.; North-Holland: New York, 1985.

(28) Dronskowski, R.; Blöchl, P. *J. Phys. Chem.* **1993**, *97*, 8617−8624.

(29) *Pearson's Handbook of Crystallographic Data for Intermetallic Phases*, 2nd ed.; Villars, P.; Calvert, L. D., Eds.; American Society for Metals: Materials Park, OH, 1991.

(30) Xie, Q.-X.; Nesper, R. *Z. Kristallogr.* **2004**, *219*, 81−82.

(31) (a) Hohnke, D.; Parthé, E. *Acta Crystallogr.* **1966**, *20*, 572−582. (b) Buschow, K. H. J.; Fast, J. F. *Phys. Status Solidi* **1966**, *16*, 467−473. (c) Eremenko, V. N.; Meleshevich, K. A.; Buyanov, Yu. I.; Martsenyuk, P. S. *Sov. Powder Metall. Met. Ceram.* **1989**, *28*, 543−547.

(32) Shoemaker, C. B.; Shoemaker, D. P. *Acta Crystallogr.* **1965**, *18*, 900−905.

(33) Pauling, L. *The Nature of the Chemical Bond*; Cornell University Press: Ithaca, NY, 1960.

(34) Bobev, S.; Bauer, E. D.; Thompson, J. D.; Sarrao, J. L.; Miller, G. J.; Eck, B.; Dronskowski, R. *J. Solid State Chem.* **2004**, *177*, 3545−3552.

(35) Vaughey, J. T.; Miller, G. J.; Gravelle, S.; Leon-Escamilla, E. A.; Corbett, J. D. *J. Solid State Chem.* **1997**, *123*, 501−507, and the references therein.

(36) (a) Leo Escamilla, E. A.; Corbett, J. D. *J. Solid State Chem.* **2001**, *159*, 149−162. (b) Mudring, A.-V.; Corbett, J. D. *J. Am. Chem. Soc.* **2004**, *126*, 5277−5281.
(37) (a) Guloy, A. M. Polar Intermetallics and Zintl Phases along the Zintl Border. In *Inorganic Chemistry in Focus III*; Wiley-VCH Verlag GmbH & Co. KGaA: Weinheim, Germany, 2006. (b) *Chemistry, Structure and Bonding of Zintl Phases and Ions*; Kauzlarich, S. M., Ed.; VCH: Weinheim, Germany, 1996, and references therein.
(38) Eckerlin, B.; Meyer, H. J.; Woelfel, E. *Z. Anorg. Allg. Chem.* **1955**, *281*, 322−328.
(39) Merlo, F.; Fornasini, M. L. *J. Less-Commom Met.* **1967**, *13*, 603−610.
(40) (a) Smart, J. S. *Effective Field Theories of Magnetism*; Saunders, Philadelphia, PA, 1966. (b) Kittel, C. *Introduction to Solid State Physics*, 7th ed.; John Wiley and Sons: Hoboken, NJ, 1996.
(41) VanVleck, J. H. *The Theory of Electric and Magnetic Susceptibilities*; Oxford University Press: London, U.K., 1965.
(42) The magnetic response for $PrLiGe_2$ in the ZFC measurement (Supporting Information), shows a cusp-like feature, which might suggest possible antiferromagnetic correlations in this compound as well.